

$^{206}\text{Pb} + n$ resonances for $E = 25\text{--}600$ keV: s -, p -, and d -wave doorway states and $M1$ ground-state radiative strength in ^{207}Pb

D. J. Horen, J. A. Harvey, and N. W. Hill

Oak Ridge National Laboratory, Oak Ridge, Tennessee 37830

(Received 20 March 1979)

High resolution neutron transmission and differential scattering measurements have been performed on ^{206}Pb and the results for $E = 25\text{--}600$ keV are presented. Data analyses were performed utilizing multilevel R -matrix codes. Resonance parameters (i.e., E , l , J , and Γ_n) were deduced for a large fraction of the 223 resonances observed. In addition to the previously known doorway in the s -wave channel, the p -wave neutron strength function exhibits significant changes near 40 and 145 keV indicative of doorway states in the $p_{1/2}$ and $p_{3/2}$ channels, respectively. These results are in good agreement with those observed in a study of the $^{207}\text{Pb} + n$ reaction. It is suggested that these doorway states arise from a $(d_{5/2}, 3^-)$ particle-core excitation. The d -wave strength function shows indications of a doorway at about $E = 425$ keV. The latter represents doorway resonances in the $d_{3/2}$ and $d_{5/2}$ channels which probably arise from a recoupling of the particle-core excitation that has been used to explain the s -wave doorway. A cumulative plot of the number of s -wave resonances vs E shows considerable curvature which indicates an increase of about 12% in the level density per 100 keV of excitation. These data were analyzed in terms of a constant temperature model with a nuclear temperature of about 0.9 MeV. The model reproduced the cumulative plot of d -wave resonances reasonably well up to $E \approx 500$ keV, but underestimated the number of p -wave resonances. This indicates a parity dependence of the level density formula for this nucleus. Many of the resonances which had previously been thought to contribute to the ground-state $M1$ radiative strength are in fact formed by s and d waves, and hence, decay by $E1$ radiation. We deduce a considerably smaller amount of $M1$ radiation for $E_x = 6738\text{--}7340$ keV in ^{207}Pb than had been reported earlier.

NUCLEAR REACTIONS $^{206}\text{Pb}(n)$, (n,n) , $E = 25\text{--}600$ keV; measured $\sigma_T(E)$, $\sigma(E, \theta)$. ^{207}Pb deduced doorway states, resonance parameters, J^π , Γ_n , neutron strength functions, level densities, $M1$ ground-state radiative strength.

I. INTRODUCTION

Detailed studies of the unbound region of heavy nuclei have been hampered because of a lack of measurements with experimental resolutions sufficient to resolve individual levels. Recently it has been shown¹⁻⁴ how high resolution neutron transmission and scattering measurements on ^{207}Pb have been able to clarify the question of $M1$ ground-state radiative strength in ^{208}Pb . Reference 3 also provided information on doorway states in the neutron entrance channel, as well as neutron strength functions for resonances with given (l, J) . For $^{207}\text{Pb} + n$, a doorway state was found in the p -wave, $J = 1^+$ channel with indications of a doorway in the $J = 2^+$ channel in the same energy interval. Such a correlation would suggest a resonance in the $p_{3/2}$ channel which should exhibit itself in the $^{206}\text{Pb} + n$ reaction.

The present work was undertaken to search for doorway states in the $^{206}\text{Pb} + n$ reaction common to those observed for ^{207}Pb , as well as to seek clarification of the $M1$ ground-state radiative strength reported by Medsker and Jackson⁵ in a study of the $^{207}\text{Pb}(\gamma, n)$ reaction. Previous measurements⁶⁻⁸ of neutron transmission by ^{206}Pb have

been rather limited and performed with poor experimental resolution. However, Farrell *et al.*⁸ reported a doorway state in the s -wave channel which was shown to be correlated with similar doorway states in other lead isotopes. Some results^{7,9,10} of resonance neutron capture on ^{206}Pb have been reported in the literature, as well as other $^{207}\text{Pb}(\gamma, n)$ data.¹¹⁻¹³ Here we report neutron resonance parameters for the energy interval $E_n = 25\text{--}605$ keV, and offer a reinterpretation of the $^{207}\text{Pb}(\gamma, n)$ work⁵ of Medsker and Jackson.

II. EXPERIMENTAL

The experimental procedures used here were similar to those described^{3,4} previously. Electrons were accelerated in bursts of 5-ns duration with a repetition rate of 800 s⁻¹ to an energy of 140 MeV with the Oak Ridge Electron Linear Accelerator (ORELA), and allowed to strike a Be-clad, water-moderated tantalum target. This produces a "white" neutron spectrum which peaks at about 1 MeV.

For the transmission measurements, filters of 3.0 cm of uranium and 0.3 g/cm² ^{10}B were inserted prior to the lead sample in order to reduce

the γ flash at the detector and to eliminate the overlap of low-energy neutrons from following bursts. The neutron beam was collimated onto either a 3.45-cm diameter cylinder of radiogenic lead (88.38% ^{206}Pb) or a sample consisting of a combination of natural lead (0.168 cm thick) and enriched (92.4%) ^{207}Pb (0.284 cm thick). The latter combination was chosen so as to compensate for the $^{207,208}\text{Pb}$ content in the sample of radiogenic lead and thus provide a transmission measurement for an effectively pure sample of ^{206}Pb (i.e., <99.5%) with a thickness of $n = 0.0989$ atoms/b. For the energy region below $E_n = 70$ keV (except for the 3.35-keV resonance), a noncompensated sample of radiogenic lead which had $n = 0.0257$ atoms/b was used. The lead samples were placed 9 m from the neutron source and the transmitted neutrons were detected at 200.252 m by means of a 7.62-cm diameter by 2.0-cm thick NE-110 plastic scintillator mounted upon an RCA-4522 photomultiplier. The neutron detector was

located in air near the center of an evacuated 122-cm diameter scattering chamber by means of a re-entrant tube which had a thin Mylar window. Details of the methods employed at ORELA by which data are accumulated corrected for various backgrounds and reduced to transmission spectra can be found in Ref. 14 and will not be restated here. The reduced data for $E_n = 85\text{--}605$ keV are plotted as total cross sections in Figs. 1–8.

The scattering measurements were also made at the 200-m flight station. The sample consisted of a hollow cylinder of radiogenic lead 6.35 cm long with a 3.18-cm outer diameter and 0.254-cm wall thickness, and was suspended at the center of the scattering chamber by means of a fine wire. Data were recorded simultaneously at three angles. Each neutron detector consisted of a 10.2-cm long by 4.32-cm diameter cylinder of NE-110 mounted upon an RCA8850 photomultiplier tube which was situated in air and encased in a thin walled steel housing. The sample to detector

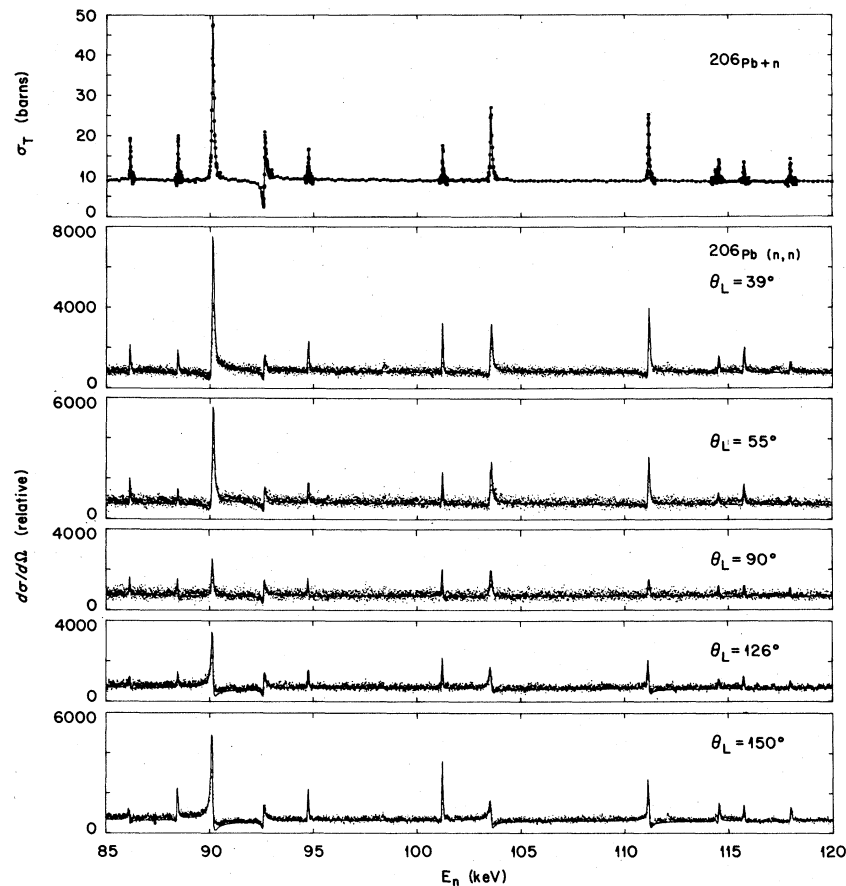


FIG. 1. Total (top) and differential elastic scattering cross sections at 39° , 55° , 90° , 126° , and 150° for $^{206}\text{Pb} + n$ reaction for $E = 85\text{--}120$ keV. The data are represented by the points and the calculated curves by the solid lines. The total cross section is for an effectively pure ^{206}Pb sample while the differential data are for radiogenic lead. See text for discussion of the R -matrix fit to σ_T and calculations of $\sigma(E, \theta)$ as well as normalization of the latter with the data.

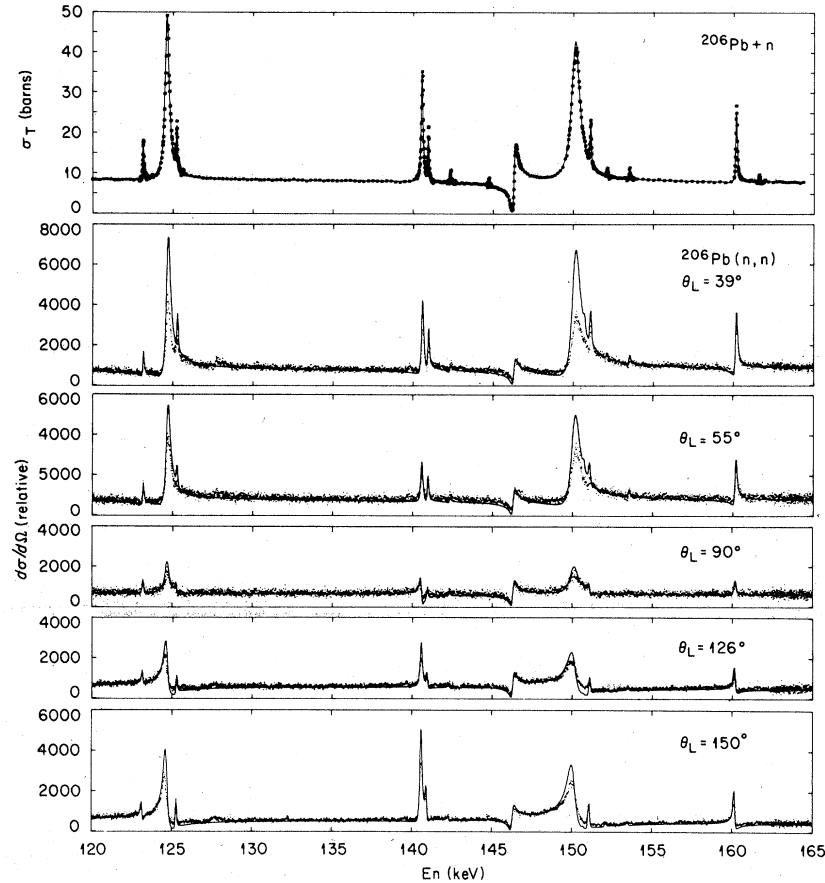


FIG. 2. Total (top) and differential elastic scattering cross sections at 39° , 55° , 90° , 126° , and 150° for $^{206}\text{Pb}+n$ reaction for $E=120\text{--}165$ keV. The data are represented by the points and the calculated curves by the solid lines. The total cross section is for an effectively pure ^{206}Pb sample while the differential data are for radiogenic lead. See text for discussion of the R -matrix fit to σ_T and calculations of $\sigma(E, \theta)$ as well as normalization of the latter with the data.

distance (i.e., center to center) was 17.8 cm. The relative efficiencies of the three detectors were shown to be similar by comparison of their spectra accumulated at the same angle for a given neutron flux. Measurements were made at laboratory angles of 39° , 55° , 90° , 126° , and 150° . The effects due to scattering by the residual air and chamber walls and detector-detector scattering were found to be small, as was the estimated multiple scattering in the sample. However, the effects of attenuation in the sample were evident for resonances with large peak cross sections.

The scattering data were recorded in two runs with the three detectors first positioned at 39° , 90° , and 150° and then 55° , 90° , and 126° . The two runs were normalized by means of the detector which was positioned at 90° . In order to reduce the data to relative differential cross sections, we proceeded as follows. A time of flight

spectrum was recorded in one of the detectors which was exposed directly to the incident neutron flux (with ORELA run at reduced power). The yield in this case was proportional to the product of the incident neutron flux and detector efficiency, i.e., $F(E)\epsilon(E)$. After dividing this spectrum into each of the lead spectra, the latter were then proportional to $\sigma(E, \theta)$ (except for sample thickness effects as noted above) and these are shown in Figs. 1–8.

From the transmission data it was found that the overall energy resolution could be represented by the expression $(\Delta E/E)^2 = a + bE$, where ΔE is the full width at half maximum (FWHM) and a and b are 0.20×10^{-6} and $(0.47 \times 10^{-6} \text{ MeV}^{-1})$, respectively.

III. DATA ANALYSIS

The transmission data were analyzed with an R -matrix¹⁵ least squares fitting program¹⁶ MULTI

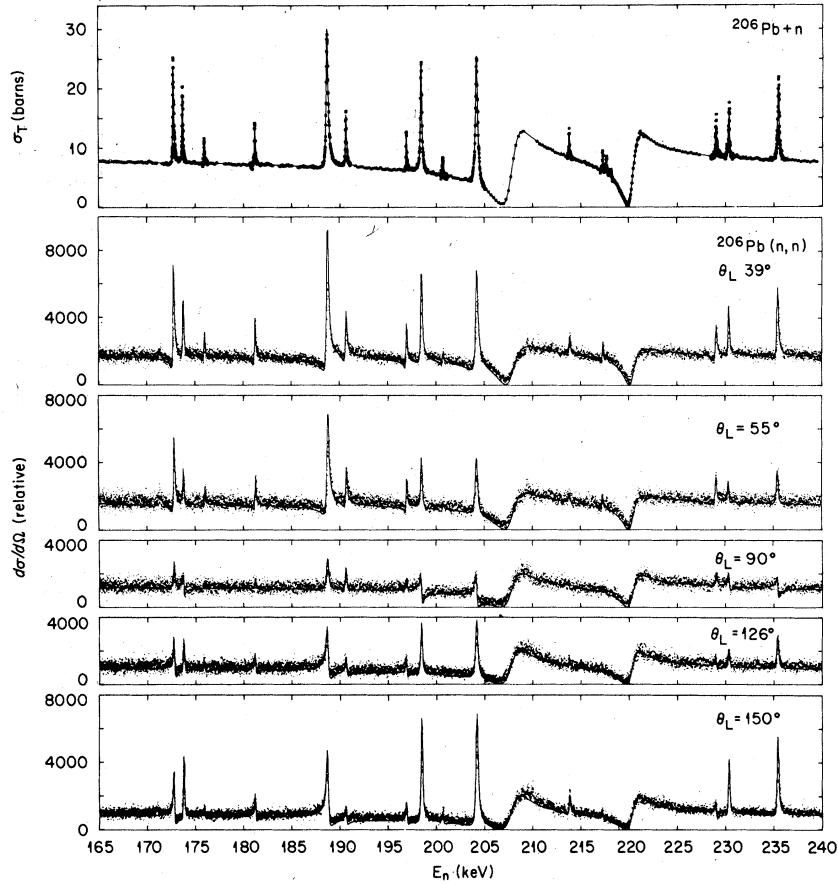


FIG. 3. Total (top) and differential elastic scattering cross sections at 39° , 55° , 90° , 126° , and 150° for $^{206}\text{Pb} + n$ reaction for $E = 165\text{--}240$ keV. The data are represented by the points and the calculated curves by the solid lines. The total cross section is for an effectively pure ^{206}Pb sample while the differential data are for radiogenic lead. See text for discussion of the R -matrix fit to σ_T and calculations of $\sigma(E, \theta)$ as well as normalization of the latter with the data.

which folds in the Doppler broadening and experimental energy resolution. The cross section is expressed as

$$\sigma_T = \sum \sigma_{nT} = 2\pi\lambda^2 \sum_J g(J) \text{Re}(1 - U_{nn}^J),$$

$$U_{nn}^J = e^{-2i\phi_l} \frac{1 - R_l^J(S_l - B_l^J - iP_l)}{1 - R_l^J(S_l - B_l^J + iP_l)},$$

$$R_l^J = \sum_\lambda \frac{\gamma_{l\lambda}\gamma_{l\lambda}}{E_\lambda - E - i\Gamma_{\gamma\lambda}/2}.$$

Here R_l^J is the R matrix, $2\pi\lambda$ is the neutron wave length, assuming that the only open channels are elastic neutron scattering and photon emission, $\gamma_{l\lambda}$ and $\Gamma_{\gamma\lambda}$ are the neutron reduced width amplitude and the radiation width, respectively, for the λ th resonance. The ϕ_l , S_l , B_l , and P_l represent the usual hard sphere phase shifts, shift factors,

boundary conditions, and penetration factors, respectively. For this work we set $B_l^J = S_l$, and assumed that the radiation widths were negligible in comparison with the neutron widths.

Differential elastic scattering cross sections were also calculated by means of an R -matrix code¹⁷ using the formalism¹⁸ of Blatt and Biedenharn. For spin zero targets, the differential cross section can be written as

$$\sigma(E, \theta) = \lambda^2 \sum_L B_L P_L(\theta),$$

where $P_L(\theta)$ are Legendre polynomials and B_L are coefficients which are functions of the phase shifts,

$$i_J = -\phi_l + \arctan \left[\frac{P_l R_l^J}{1 - R_l^J(S_l - B_l^J)} \right].$$

The center of mass cross sections were translated to the laboratory system and "smeared" to account

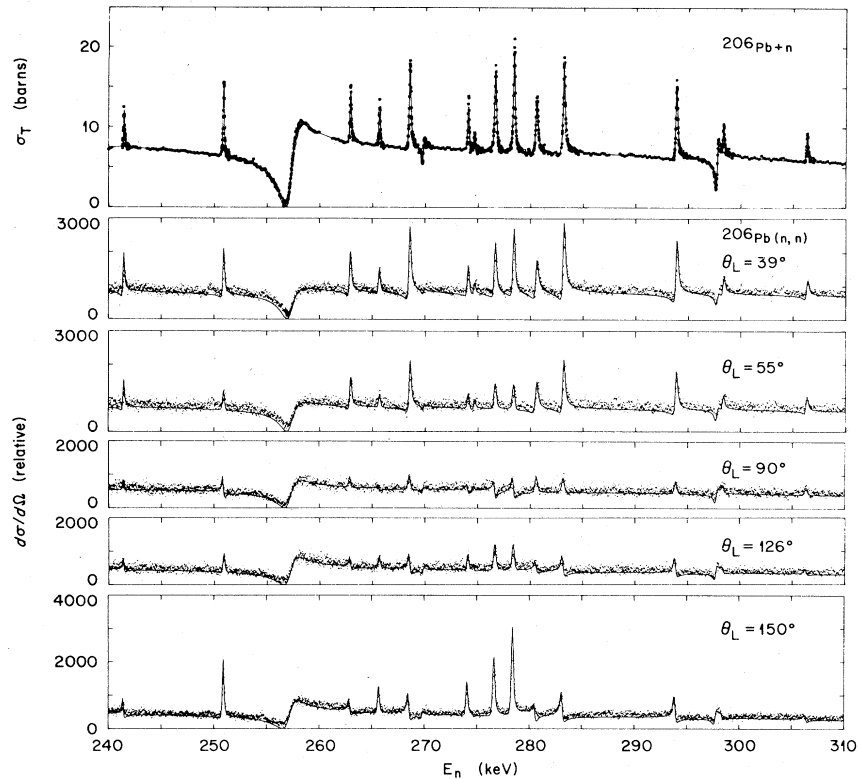


FIG. 4. Total (top) and differential elastic scattering cross sections at 39°, 55°, 90°, 126°, and 150° for $^{206}\text{Pb}+n$ reaction for $E=240\text{--}310$ keV. The data are represented by the points and the calculated curves by the solid lines. The total cross section is for an effectively pure ^{206}Pb sample while the differential data are for radiogenic lead. See text for discussion of the R -matrix fit to σ_T and calculations of $\sigma(E, \theta)$ as well as normalization of the latter with the data.

for the experimental energy resolution by means of programs¹⁹ developed by Kinney.

Usually, one can easily recognize an s -wave resonance by its large interference pattern in the total cross section spectrum. For many resonances, an inspection of the shape in the scattering spectra was sufficient to assign an l value. For example, p waves exhibit an interference pattern which rises rapidly on the low-energy side and falls off slowly on the high-energy side for scattering in the forward hemisphere, reverses itself in the backward hemisphere, and is symmetric at 90°. At the lower energies one can also distinguish between $p_{1/2}$ and $p_{3/2}$ by examining the change in magnitude of the cross section with angle. For $p_{3/2}$ resonances $\sigma(E, \theta)$ is larger at angles of 126° and 150° than at 90°, while the contrary is true for $p_{1/2}$ resonances. The $l=2$ resonances have larger $\sigma(E, \theta)$ at 150° than at 39°, and in general show strong interference at 90°.

For most of the resonances with $\Gamma_n \gtrsim \Delta E$ (i.e., the energy resolution) we were able to determine

the l values (and sometimes J) from the scattering data. The l, J were then held fixed when using MULTI to fit the transmission data. In using MULTI, we fixed the nuclear radius at 8.042 fm and placed "dummy" resonance far from the region to be analyzed to account for "far removed resonances." We used an iterative approach for analysis of the transmission spectrum between $E_n = 25\text{--}605$ keV. The data were first analyzed in the energy interval $E = 20\text{--}700$ keV to obtain approximate values of the parameters for the s wave as well as dummy resonances. The dummy resonances were located at -4 MeV for s and d waves and at 8 MeV for p waves. The energy region under consideration was then broken up into approximately 100–200 keV intervals (depending upon the density of resonances) for analysis using MULTI. This program is capable of calculating cross sections with parameters for approximately 100 resonances. Parameter files were made for each energy interval. In general, each file contained fixed parameters for resonances adjacent to the lower and upper boundaries

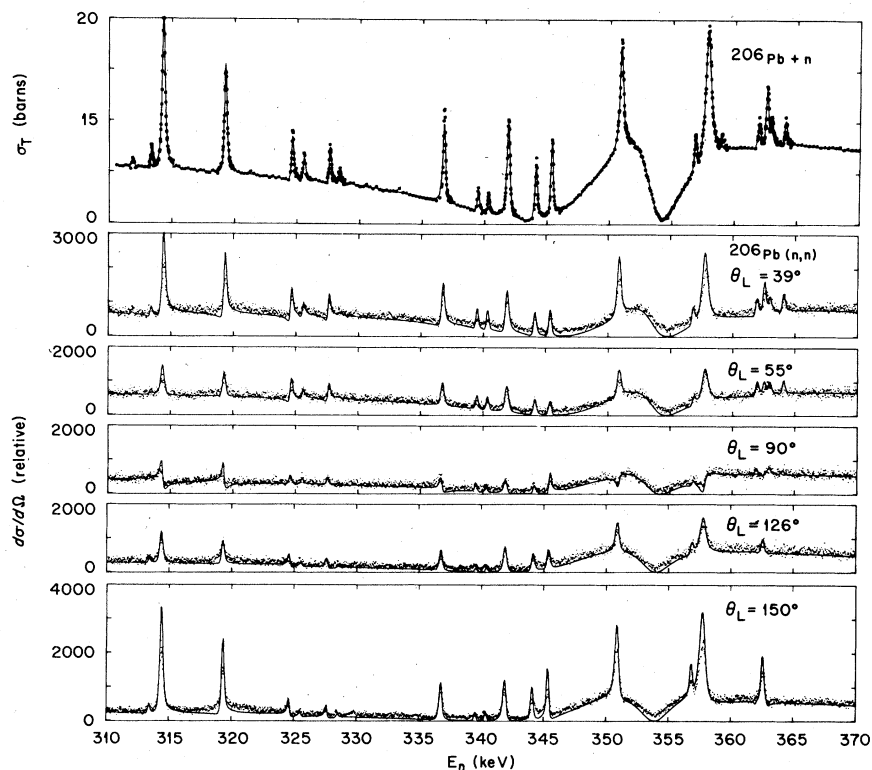


FIG. 5. Total (top) and differential elastic scattering cross sections at 39° , 55° , 90° , 126° , and 150° for $^{206}\text{Pb} + n$ reaction for $E = 310 - 370$ keV. The data are represented by the points and the calculated curves by the solid lines. The total cross section is for an effectively pure ^{206}Pb sample while the differential data are for radiogenic lead. See text for discussion of the R -matrix fit to σ_T and calculations of $\sigma(E, \theta)$ as well as normalization of the latter with the data.

(to account for the contribution of nearby resonances to the region being analyzed), parameters to be varied for each resonance within the interval, parameters for all of the known s -wave resonances outside the interval, and parameters for the dummy resonances. For the latter, the energies were held fixed and the widths allowed to vary. After several iterations it was found that the data could be fitted reasonably well over the range $E_n = 85 - 605$ keV with the same set of widths for the dummy resonances. Parameters for the dummy resonances were as follows: $s_{1/2}$ ($E = -4$ MeV, $\Gamma_n = 5$ MeV), $p_{1/2}$ ($E = 8$ MeV, $\Gamma_n = 12$ MeV), $p_{3/2}$ ($E = 8$ MeV, $\Gamma_n = 12$ MeV), $d_{3/2}$ ($E = -4$ MeV, $\Gamma_n = 2$ MeV), and $d_{5/2}$ ($E = -4$ MeV, $\Gamma_n = 2$ MeV). Final fits to the total cross section (i.e., transmission) data are shown by the solid curves through the experimental points in the upper curves in Figs. 1-8, and the resonance parameters are given in Table I. This table also includes the energies of a number of small resonances which we did not include in our analysis.

After demonstrating that this parameter set used with the code for calculating differential elastic

scattering cross sections reproduced the observed total cross section we used it to calculate $\sigma(E, \theta)$ at each angle. As mentioned previously, the experimental resolution was taken into account in these calculations. The experimental spectra were scaled so that the calculated curve in regions void of resonances (i.e., differential cross section mainly due to potential scattering) accounted for about 88% of the relative cross section (i.e., the remaining 12% arising from the other lead isotopes in the sample). The results are shown by the solid curves in the differential scattering spectra in Figs. 1-8; the points represent the experimental data. In these figures it can be seen that the calculated cross sections are larger than the experimental values for many of the resonances which have large peak cross sections, and, as mentioned earlier, this is due to attenuation in the sample. The data have not been corrected for this effect. Although the differential cross sections are shown as relative in Figs. 1-8, the scales correspond to the calculated cross sections in mb/sr and represent predictions of the absolute differential elastic cross sections.

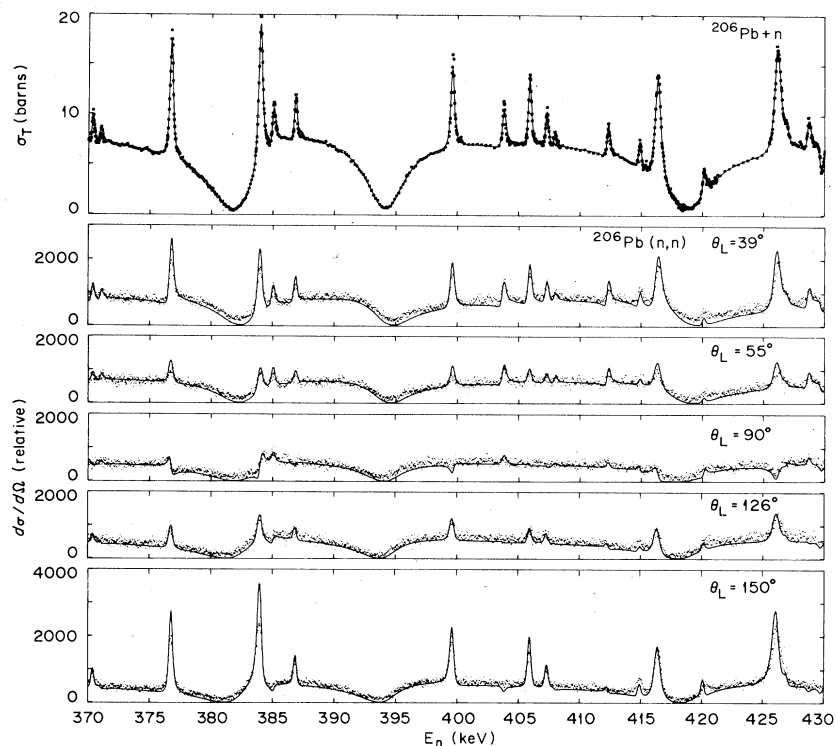


FIG. 6. Total (top) and differential elastic scattering cross sections at 39° , 55° , 90° , 126° , and 150° for $^{206}\text{Pb}+n$ reaction for $E=370\text{--}430$ keV. The data are represented by the points and the calculated curves by the solid lines. The total cross section is for an effectively pure ^{206}Pb sample while the differential data are for radiogenic lead. See text for discussion of the R -matrix fit to σ_T and calculations of $\sigma(E, \theta)$ as well as normalization of the latter with the data.

The agreement between the calculated and experimental spectra in Figs. 1–8 indicates the degree of confidence in the assigned parameters. Resonance parameters for which unique assignments could not be made are enclosed in parentheses in Table I. It should be noted that the tabulated neutron widths are correlated with the assigned J values and must be adjusted if the corresponding J values are changed.

No attempt will be made here to make a detailed comparison with previously reported results from transmission measurements. As will be apparent later, our s -wave parameters are in general agreement with those found by Farrell *et al.*⁹

IV. DISCUSSION

Strength functions and doorway states for $l=0$ resonances. In Fig. 9 is plotted the sum of the neutron reduced widths (Γ_n^0) versus neutron energy for the s -wave resonances. Here Γ_n^i is the reduced neutron width defined as

$$\Gamma_n^i = \frac{\Gamma_n(1 \text{ eV})^{1/2}}{v_i(E)^{1/2}}$$

where Γ_n and E are given in electron volts and v_i is the penetration factor for a neutron having angular momentum l . As mentioned earlier, our results for the s -wave resonances are in general agreement with those of Farrell *et al.*⁸ Our energies and reduced widths are slightly different and we observe a few more resonances in the 25–605 keV interval. However, this is not surprising in view of our much better experimental energy resolution.

The increase in the strength function (i.e., slope of the curve) seen in Fig. 9 was suggested by Farrell *et al.*⁸ as arising from a possible doorway state which was common²⁰ to the $^{207,208,209}\text{Pb}$ compound nuclear systems. Beres and Divadeenam²¹ have described this doorway state in terms of a $(2g_{3/2}, 4^+)$ particle-core excitation.

$l=1$ resonances. It was difficult to distinguish between $p_{1/2}$ and $p_{3/2}$ resonances above about 350 keV and thus the tabulated J and Γ_n values in that region are to be considered as tentative. However, the product $g\Gamma_n$ is essentially independent of the assumed J value. In Fig. 10 are shown plots of the sum of the reduced neutron widths for p

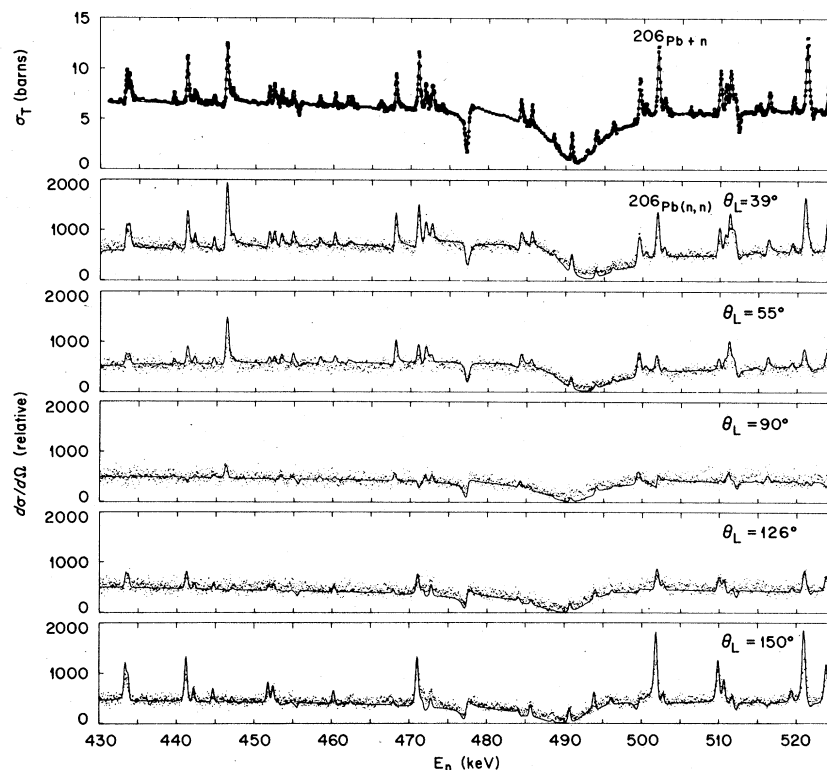


FIG. 7. Total (top) and differential elastic scattering cross sections at 39° , 55° , 90° , 126° , and 150° for $^{206}\text{Pb} + n$ reaction for $E = 430\text{--}520$ keV. The data are represented by the points and the calculated curves by the solid lines. The total cross section is for an effectively pure ^{206}Pb sample while the differential data are for radiogenic lead. See text for discussion of the R -matrix fit to σ_T and calculations of $\sigma(E, \theta)$ as well as normalization of the latter with the data.

waves. For the region below 350 keV we show separate plots for the $p_{1/2}$ and $p_{3/2}$ channels. The change in strength function near 145 keV is clearly caused by a doorway resonance in the $p_{3/2}$ channel and the change near 40 keV by a doorway resonance in the $p_{1/2}$ channel. Below 47.5 keV, Mizumoto *et al.*²² observed thirteen additional resonances of which they suggest seven are most likely p wave. They report a p -wave strength function of $S_1 \approx 1.7 \times 10^{-5}$ below 25 keV, and $S_1 \approx 16 \times 10^{-5}$ in the region of the $p_{1/2}$ doorway.

The doorway near 145 keV occurs at nearly the same neutron energy as that^{1,3} observed for ^{207}Pb in the 1^+ (and 2^+) channel. Furthermore, the magnitude of the p -wave strength function within the doorway is very similar for the two reactions, i.e., $S_1 \approx 1.7 \times 10^{-4}$ vs $S_1 \approx 2.0 \times 10^{-4}$ for ^{207}Pb and ^{206}Pb , respectively. Likewise, the value above this doorway is also quite similar, $S_1 \approx 3.5 \times 10^{-5}$ vs $S_1 \approx 1.3 \times 10^{-5}$, respectively. This suggests that the origin of the doorway state is common to both reactions. We suggest that it arises from a particle-core excitation involving the $d_{5/2}$ particle and

the 3^- collective excitation. The excitation energy of the doorway in $^{206}\text{Pb} + n$ occurs at $E_x \approx 6885$ keV (i.e., $S_n + E_n$) which can be compared with an energy of $E_x \approx 7038$ keV for the $(d_{5/2}, 3^-)$ particle-core excitation (i.e., sum of the energy of the $d_{5/2}$ state in ^{207}Pb plus the 3^- state in ^{206}Pb). Similarly, for $^{207}\text{Pb} + n$ one finds the doorway at $E_x \approx 7498$ versus 7615 keV for the corresponding particle-core excitation. The concentration of the strength within only a few resonances is probably a reflection of the fact that the $d_{5/2}$ single particle strength is primarily contained in a single bound-state level in $^{207,208}\text{Pb}$ and the density of background states with which the particle-core excitation can mix is low. A test of these arguments could come from investigations of the $^{204,208}\text{Pb} + n$ reactions. All of the $d_{5/2}$ single particle strength in ^{209}Pb is reported to be in a level at 1566 keV, and the analogous doorway state would occur at $E_x \approx 4181$ keV where the level density of the background states is expected to be low. Hence, we would expect the doorway in $^{208}\text{Pb} + n$ to reveal itself in a manner similar to that for the $^{206,207}\text{Pb}$

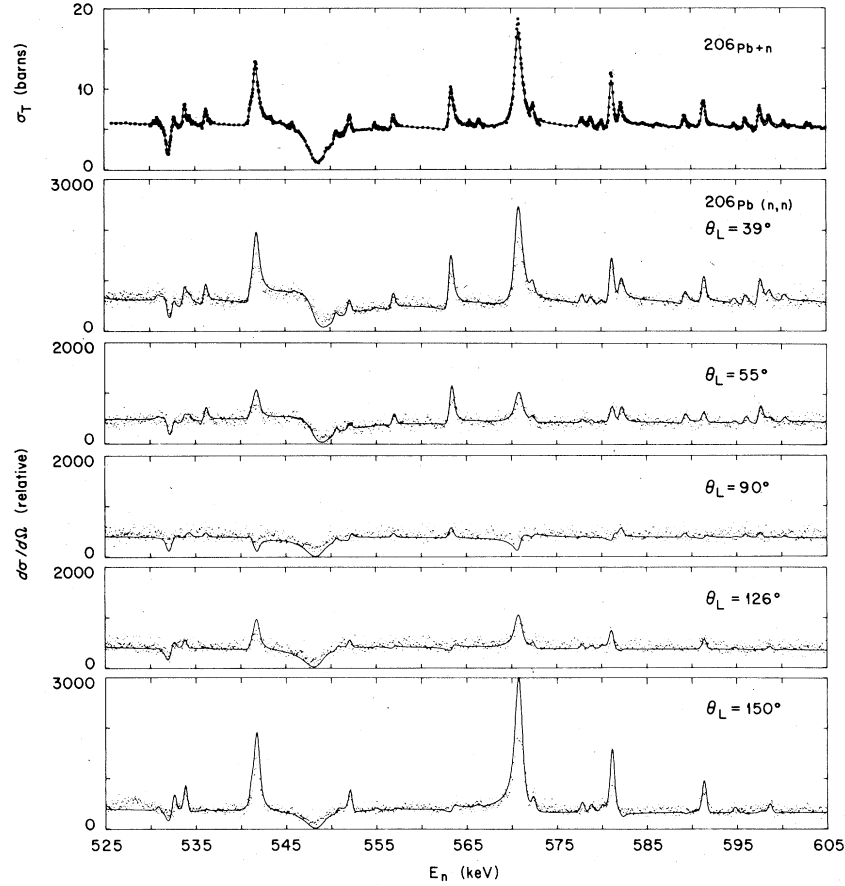


FIG. 8. Total (top) and differential elastic scattering cross sections at 39°, 55°, 90°, 126°, and 150° for $^{206}\text{Pb}+n$ reaction for $E=525\text{--}605$ keV. The data are represented by the points and the calculated curves by the solid lines. The total cross section is for an effectively pure ^{206}Pb sample while the differential data are for radiogenic lead. See text for discussion of the R -matrix fit to σ_T and calculations of $\sigma(E, \theta)$ as well as normalization of the latter with the data.

$+n$ reactions. However, in ^{205}Pb the $d_{5/2}$ strength is highly fragmented so that the strength in the doorway state should be more distributed and somewhat more difficult to detect. Investigations of the $^{204,208}\text{Pb}+n$ reactions are currently underway at ORELA in order to investigate these possibilities.

For ^{206}Pb we find $\sum(2l+1)^{-1}g\Gamma_n^l \approx 3.2$ eV for the resonances within the $p_{1/2}$ doorway. Assuming the 16.758- and 37.72-keV 1^+ resonances³ in $^{207}\text{Pb}+n$ from the analogous doorway, one finds $\sum(2l+1)^{-1}g\Gamma_n^l \approx 2.2$ eV. Applying the weak-coupling model to the ^{207}Pb compound system, coupling of a $d_{5/2}$ particle to the 3^- core would give rise to a multiplet of levels, two of which would have J^π values $\frac{1}{2}^-$ and $\frac{3}{2}^-$. Using the weak-coupling particle-vibration model of Divadeenam and Beres²¹ for a target with spin zero, the neutron width is given by

$$\Gamma_n^J = \frac{Km}{(2\pi)^2 \hbar^2} \sum_{m_s} \int d\Omega_K |\langle X_J | V_c | 0^+, \chi^{(*)}(K, m_s) \rangle|^2,$$

where K is the wave number related to the energy by $E = \hbar^2 K^2 / 2m$, m is the neutron reduced mass, and m_s is the z projection of the intrinsic spin. The unperturbed particle-vibration state $\langle (3d_{5/2}, 3^-) J$ is designated by X_J , and $\chi^{(*)}(K, m_s)$ represents the wave function of the outgoing neutron. The coupling interaction is given by

$$V_c = k(r)(2\lambda + 1)^{1/2}(\alpha Y_\lambda)_0,$$

where

$$k(r) = -r \frac{dV(r)}{dr}.$$

Here $V(r)$ is the real radial one-body potential. Upon substitution of V_c into the expression for Γ_n^J , the latter can be written as the product of rad-

TABLE I. Resonance parameters for the $^{206}\text{Pb} + n$ reaction. Ground-state radiation widths for the $^{207}\text{Pb}(\gamma, n)$ reaction reported in Ref. 5 are also tabulated.

$^{206}\text{Pb} + n^a$					$^{207}\text{Pb}(\gamma, n)^b$			
E_n^c (keV)	l	J^π^d	$\Gamma_n(\text{eV})^e$	$\Gamma_n^2(\text{eV})^{e,f}$	E_γ^g (keV)	$g_\gamma \Gamma_\gamma \Gamma_n / \Gamma$ (eV)	$R(\theta = 90^\circ / \sigma_{135^\circ})$	
3.35	1	3/2 ⁻	0.25	8	0.42			
25.42	1	1/2 ⁻	51	6	4.4			
36.21	1	1/2 ⁻	40	6	2.1			
47.49	1	1/2 ⁻	89	10	3.2			
53.90	1	3/2 ⁻	6.2	14	0.19			
59.23	(2)							
63.95	(2)		[3] ^h		[2.9]			
65.99	0	1/2 ⁺	85	9	0.33	65.6	0.9	0.91 10
66.59	1	3/2 ⁻	10	2	0.22			
70.28	1	1/2 ⁻	10	3	0.20			
78.2±0.2	1	3/2 ⁻	(11) ^h		(0.20)			
80.36	2	3/2 ⁺	[7] ^h		[3.5]			
82.70	1	(1/2) ⁻						
82.92	2		[16] ^h		[8.3]			
86.13	1	1/2 ⁻	16	4	0.27	83.6	0.11	1.30 35
88.45	2	5/2 ⁺	8	3	3.6			
90.13	1	3/2 ⁻	75	8	1.2			
92.62	0	1/2 ⁺	32	5	0.10	92.9	0.8	0.84 14
94.76	2	(3/2) ⁺	7	2	2.7			
101.22	2	(5/2) ⁺	8	2	2.5			
103.56	1	1/2 ⁻	65	8	0.84			
111.17	1	3/2 ⁻	30	4	0.35			
114.39	(1)	(3/2) ⁻	2.5	7	0.029			
114.55	2	(5/2) ⁺	5.6	11	1.4	115.1	0.33	1.18 27
115.76	1	(3/2) ⁻	5.7	11	0.064			
117.99	2	(5/2) ⁺	5.1	12	1.1			
123.16	1	1/2 ⁻	35	5	0.36			
124.65	1	3/2 ⁻	300	25	3.06	124.2	5.4	1.14 7
125.25	2	(3/2) ⁺	21	4	4.1			
140.57	2	3/2 ⁺	103	15	15.3	140.3	2.1	1.23 10
140.95	1	3/2 ⁻	28	5	0.25			
142.33	1	1/2 ⁻	12	2	0.10			
144.73	(2)	(3/2) ⁺	3.1	10	0.44			
146.31	0	1/2 ⁺	176	15	0.46	146.4	2.5	0.91 8
150.11	1	3/2 ⁻	598	25	4.87			
150.70	(1)	(1/2) ⁻	4.4	15	0.04			
151.09	2	5/2 ⁺	19	3	2.3			
152.12	(2)	(5/2) ⁺	0.5	2	0.06			
153.52	1	(1/2) ⁻	10	3	0.077			
160.17	1	3/2 ⁻	68	7	0.52			
161.59	(2)	(5/2) ⁺	0.6	2	0.07			
171.33						169.6	0.31	1.31 25
172.78	1	3/2 ⁻	73	8	0.50			
173.74	2	(3/2) ⁺	47	5	4.3	173.7	0.3	0.89 16
175.96	1	3/2 ⁻	13	4	0.09	176.7	0.28	1.37 29
177.66								
181.23	1	3/2 ⁻	27	6	0.18			
183.25								
185.52								
188.73	1	3/2 ⁻	200	20	1.25			
190.66	1	1/2 ⁻	97	13	0.60			
191.32								
196.92	1	1/2 ⁻	64	15	0.38			
198.47	2	3/2 ⁺	132	17	8.8	198.9	4.0	0.99 6
200.69	1	3/2 ⁻	12	3	0.069			
204.21	2	3/2 ⁺	235	25	14.7	204.0	0.25	0.94 11
207.89	0	1/2 ⁺	2173	100	4.77			
209.41								
209.97								
213.83	2	(3/2) ⁺	22	5	1.3			
217.30	1	3/2 ⁻	10	3	0.055			
217.67	1	1/2 ⁻	22	7	0.12	217.1	0.3	0.89 9
218.16	(1)	(1/2) ⁻	6.2	2	0.033	218.5	0.2	0.95 13
220.43	0	1/2 ⁺	1407	80	3.00			
227.81						228.2	0.4	1.12 10
229.03	1	3/2 ⁻	35	5	0.18			
230.37	2	5/2 ⁺	40	7	1.9			
235.47	2	3/2 ⁺	107	12	4.9	235.3	1.4	1.36 9
241.42	1	3/2 ⁻	39	7	0.19			
242.3						242.3	0.7	1.28 30
243.30								
250.88	2	5/2 ⁺	52	8	0.19	254.4	0.09	0.83 13
254.6								
257.28	0	1/2 ⁺	1427	90	2.81	258.5	0.4	1.20 15
260.36								
260.78								
262.88	1	3/2 ⁻	54	8	0.24	262.5	0.8	1.31 19
265.63	2	3/2 ⁺	40	7	1.4	265.5	0.5	1.28 20
268.50	1	3/2 ⁻	106	13	0.45			
269.77	0	1/2 ⁺	31	6	0.06	269.6	0.8	(2.03)
274.06	2	(3/2) ⁺	53	8	1.7			

TABLE I. (Continued)

206Pb + n ^a						207Pb(γ , n) ^b			
E _n ^c (keV)	λ	J π ^d	Γ_n (eV) ^e		Γ_n^s (eV) ^{e, f}	E _g (keV)	$g\gamma\Gamma_{\gamma 0}\Gamma_n/\Gamma$ (eV)	R($\sigma_{90^\circ}/\sigma_{135^\circ}$)	
274.63	1	(1/2) ⁻	32	6	0.13				
276.63	2	3/2 ⁺	112	14	3.6	276.7	4.0	1.09	10
278.40	2	5/2 ⁺	100	12	3.2				
280.54	1	1/2 ⁻	171	18	0.70	280.7	0.7	1.28	30
283.13	1	3/2 ⁻	133	14	0.54				
287.95	(1)								
289.25									
289.66									
293.85	1	3/2 ⁻	110	12	0.43	291.8	0.7	1.38	18
297.71	0	1/2 ⁺	113	12	0.21				
298.34	1	(1/2) ⁻	62	9	0.24				
306.30	1	1/2 ⁻	73	8	0.27	299.9	1.5	1.23	11
311.88	(2)	(5/2 ⁺)	2.2	9	0.06	308.0	0.5	1.43	22
313.40	2	(3/2) ⁺	22	7	0.55				
314.34	2	5/2 ⁺	179	20	4.4				
319.28	2	3/2 ⁺	164	16	3.9				
324.62	1	3/2 ⁻	55	7	0.19				
325.56	1	1/2 ⁻	49	7	0.17				
327.62	1	(3/2) ⁻	44	6	0.15				
328.48	(2)	(5/2 ⁺)	6.3	20	0.14				
336.74	2	(3/2) ⁺	128	17	2.7	336.2	0.9	1.22	12
339.50	(2)	(5/2 ⁺)	16	4	0.33				
340.34	(2)	(5/2 ⁺)	16	4	0.33				
341.89	2	3/2 ⁺	174	20	3.5	341.3	0.8	1.49	11
344.13	2	3/2 ⁺	85	11	1.7	344.3	0.8	1.04	16
345.39	2	5/2 ⁺	76	11	1.5				
347.24	0	1/2 ⁺	10980	600	18.63	347.3	1.0	1.05	24
350.91	2	3/2 ⁺	212	30	4.1	350.4	2.8	1.06	18
355.32	0	1/2 ⁺	5299	400	8.89	354.4	1.5	1.09	10
356.86	2	(5/2) ⁺	31	6	0.6				
357.83	2	3/2 ⁺	455	50	8.4				
358.99						358.4	1.4	1.39	18
361.94	1	1/2 ⁻	80	12	0.25				
362.58	2	3/2 ⁺	98	15	1.8				
362.94	(1)	(3/2) ⁻	36	5	0.12				
364.06	1	(3/2) ⁻	34	7	0.11				
370.37	2	(3/2) ⁺	45	9	0.8				
371.05	1	(1/2) ⁻	40	8	0.12	370.6	0.8	1.09	21
376.71	2	5/2 ⁺	191	25	3.2				
382.84	0	1/2 ⁺	4447	300	7.13				
383.95	2	5/2 ⁺	281	35	4.5				
385.03	1	1/2 ⁻	157	20	0.47				
386.85	2	3/2 ⁺	79	13	1.2	386.7	1.4	1.11	16
395.05	0	1/2 ⁺	4396	270	6.99				
399.60	2	(5/2) ⁺	138	21	2.0	398.8	1.0	1.30	24
403.76	1	1/2 ⁻	173	24	0.49				
405.91	2	5/2 ⁺	102	20	1.5				
407.31	2	3/2 ⁺	71	10	1.0	406.9	1.5	1.00	12
407.94	1	(1/2) ⁻	44	9	0.12				
412.30	1	1/2 ⁻	126	15	0.27				
414.88	2	3/2 ⁺	50	12	0.8	413.0	0.8	0.91	26
416.37	2	5/2 ⁺	307	40	4.2	416.0	2.6	1.17	10
419.77	0	1/2 ⁺	6363	600	9.82	419.0	1.25	1.06	14
420.14	2	(5/2) ⁺	34	7	0.5				
426.14	2	3/2 ⁺	522	60	6.8	426.1	5.8	1.25	8
426.90	(2)	(5/2 ⁺)	17	6	0.2				
428.68	1	(1/2) ⁻	128	15	0.34				
429.75	0	1/2 ⁺	129	15	0.20				
433.39	2	(5/2) ⁺	47	18	0.6				
433.74	2	(3/2) ⁺	58	20	0.7	433.2	2.1	1.13	12
439.45	(1)	(1/2) ⁻	36	11	0.10				
441.22	2	(3/2) ⁺	109	15	1.3	441.2	1.5	1.14	18
442.20	(2)	(5/2 ⁺)	14	4	0.2				
444.68	(2)	(5/2 ⁺)	11	3	0.15				
446.30	1	3/2 ⁻	177	20	0.46				
447.15	(2)	(5/2 ⁺)	12	4	0.14				
451.78	(2)	(5/2 ⁺)	36	9	0.45				
452.41	2	(3/2) ⁺	44	10	0.51	452.4	2.1	1.53	17
452.74	(2)	(5/2 ⁺)	5.5	16	0.06				
453.38	1	(1/2) ⁻	59	12	0.15				
454.80	1	(3/2) ⁻	25	7	0.062				
455.57	0	1/2 ⁺	42	7	0.062	455.4	1.2	1.12	14
458.35	(1)	(1/2) ⁻	43	15	0.11				
460.24	(2)	(5/2 ⁺)	16	5	0.2				
461.93	(1)	(3/2) ⁻	15	5	0.037				
462.41	(2)	(5/2 ⁺)	9	3	0.1				

TABLE I. (Continued)

$^{206}\text{Pb} + n^a$						$^{207}\text{Pb}(\gamma, n)^b$			
E_n^c (keV)	l	$J^{\pi d}$	$\Gamma_n(\text{eV})^e$	$I_n^h(\text{eV})^{e,f}$	g_n^g (keV)	$g_n \Gamma_{\gamma 0} \Gamma_n / \Gamma$ (eV)	$R(\sigma_{90^\circ} / \sigma_{135^\circ})$		
466.21					465.5	3.2	1.30	13	
468.08	1	$3/2^-$	90	14					
471.02	2	$(3/2)^+$	161	20	471.5	1.1	1.48	26	
471.86	1	$(3/2)^-$	62	8					
472.79	(3)	$(5/2^-)$	41	9					
474.10									
477.31	0	$1/2^+$	374	40					
484.19	1	$1/2^-$	102	12					
485.67	2	$(5/2)^+$	33	7					
488.50	(2)	$(5/2^+)$	14	4					
490.76	2	$(3/2)^+$	74	10		1.1	1.48	26	
492.60	0	$1/2^+$	9166	600					
492.86									
493.96	(2)	$(5/2^+)$	29	7					
496.13	(2)	$(3/2^+)$	19	7					
499.47	1	$1/2^-$	290	60					
500.30	(1)	$(3/2^-)$	26	6					
501.93	2	$5/2^+$	152	25					
502.81	2	$(3/2)^+$	32	8					
506.13									
507.23									
509.08									
509.93	2	$(5/2)^+$	89	15					
510.69	(2)	$(3/2^+)$	86	15					
511.22	1	$(3/2)^-$	123	15					
511.80	2	$5/2^+$	16	4					
512.30	0	$1/2^+$	160	14					
514.60	(1)	$(1/2^-)$	4.2	10					
515.05	(2)	$(5/2^+)$	6.8	15					
516.18	1	$1/2^-$	110	14					
519.42	2	$(5/2)^+$	22	6					
521.09	2	$5/2^+$	188	24					
521.86	0	$1/2^+$	55	20	521.0	2.1	0.97	11	
523.89	2	$3/2^+$	161	20					
530.84	(2)	$(5/2^+)$	18	4					
532.10	0	$1/2^+$	391	25					
532.66	(2)	$(5/2^+)$	34	7					
533.85	(2)	$(5/2^+)$	60	9					
534.30	(1)	$(1/2^-)$	62	9					
536.11	1	$(3/2)^-$	63	9					
541.15	(2)	$(5/2^+)$	31	7					
541.71	2	$(3/2)^+$	517	60					
545.79	(2)	$(5/2^+)$	7.3	20	545.2	1.1	1.36	19	
548.93	0	$1/2^+$	3099	170					
550.60	1	$(3/2)^-$	32	7	549.3	0.5	0.86	19	
552.12	2	$(5/2)^+$	52	9					
554.93	(2)	$(3/2^+)$	13	4					
556.92	1	$1/2^-$	120	18					
563.29	1	$3/2^-$	253	30					
565.31	(1)	$(1/2^-)$	14	5					
566.41	(2)	$(5/2^+)$	10	3	565.5	1.3	1.04	13	
570.83	2	$5/2^+$	790	85					
572.40	2	$(3/2)^+$	56	9	572.5	7.7	0.96	5	
577.83	(2)	$(5/2^+)$	29	6					
578.80	(2)	$(3/2^+)$	36	7					
580.00	(2)	$(3/2^+)$	23	5					
581.16	2	$(5/2)^+$	208	25					
582.14	1	$(3/2)^-$	111	10					
589.22	1	$1/2^-$	110	16					
591.39	2	$(5/2)^+$	101	15	591.7	0.9	(2.21)		
594.78	(2)	$(5/2^+)$	11	3					
595.96	1	$(1/2^-)$	84	13					
597.60	1	$(3/2)^-$	111	13	597.8	2.6	1.53	11	
598.66	2	$(5/2)^+$	29	7					
600.27	(1)	$(3/2^-)$	22	6					
602.85	(2)	$(5/2^+)$	3.5	9					
603.24	(2)	$(3/2^+)$	42	8					

a. Present work.

b. From Tables II, III and IV of reference 5.

c. Uncertainties in resonance energies are $\pm 0.03\%$ except where shown.d. Those l enclosed in parentheses indicate data not sufficient to distinguish between two possible spin values.e. Γ_n and I_n^h depend upon choice of J and must be changed accordingly if it is shown that alternate spin value is applicable. Values enclosed in square brackets are g_n^l or g_n^k , respectively. Uncertainties in Γ_n are denoted as $5.6 \text{ ll} \equiv 5.6 \pm 1.1$. (Same notation for R).

f. Reduced neutron widths (at 1 eV) calculated with a channel radius of 8.042 fm.

g. Energies from (γ, n) study converted to (n, γ) system.h. From reference 22. The latter give g_n^l and these are shown within enclosed brackets. For the 78.2- and 80.36-keV resonances we give Γ_n based upon our assigned J -value.

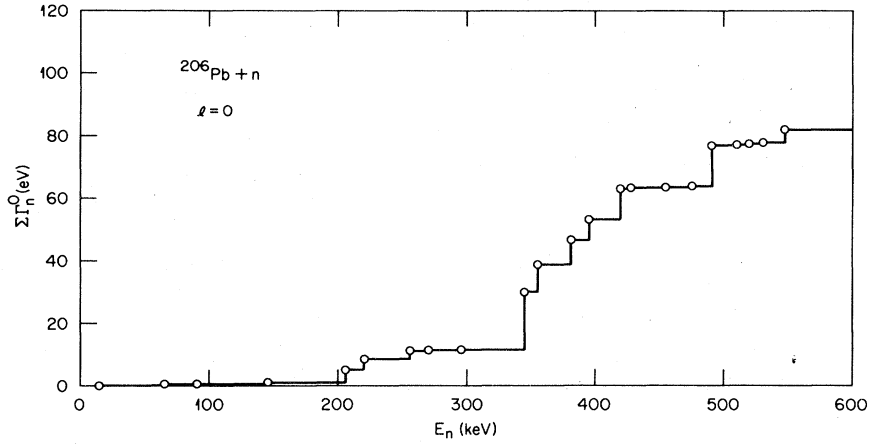


FIG. 9. Plot of the sum of the reduced neutron widths $\sum \Gamma_n^0$ for s -wave resonances versus neutron energy.

ial and angular momentum matrix elements. We assume that for a given neutron energy, the radial matrix element is independent of j , i.e., $p_{1/2}$ or $p_{3/2}$. Under these circumstances, one can easily

show that the ratio $\Gamma_n^{3/2}/\Gamma_n^{1/2}$ is proportional to the square of the ratio of the respective 3- j symbols $\begin{pmatrix} 3 & 5/2 & j \\ 0 & -1/2 & 1/2 \end{pmatrix}$. One then finds $\Gamma_n^{3/2} \approx 0.4 \Gamma_n^{1/2}$. The sums of the reduced widths within the door-

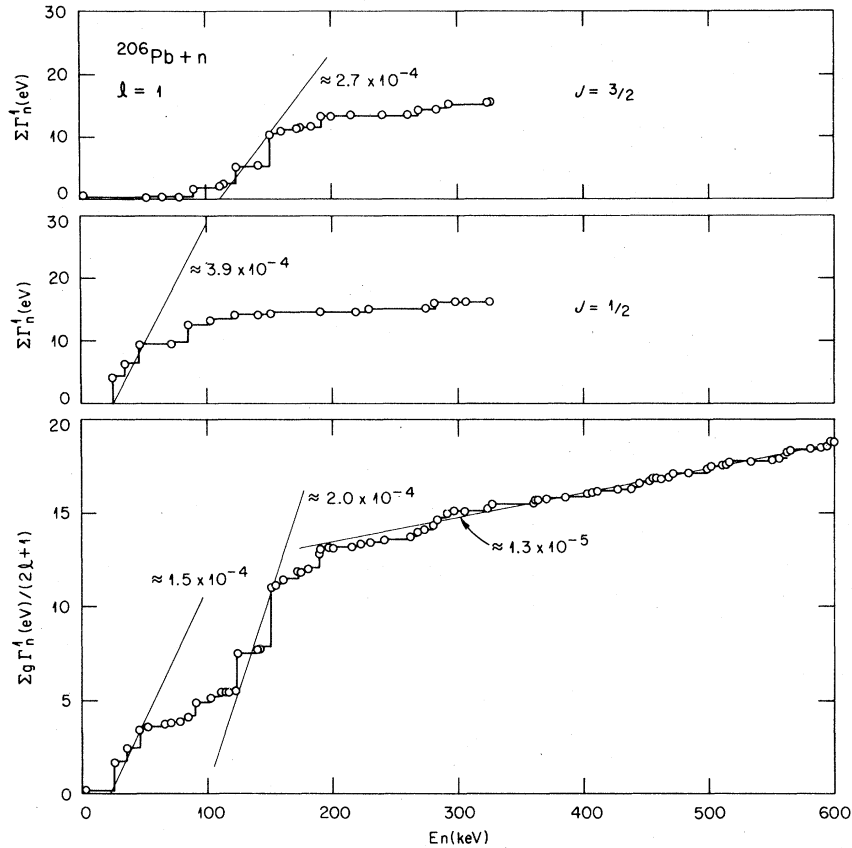


FIG. 10. Plots of the sum of reduced neutron widths $\sum \Gamma_n^1$ for p waves versus neutron energy. The top figure is for $J=3/2$ and the middle for $J=1/2$. The bottom figure is the weighted sum [i.e., $\sum g \Gamma_n^1 (2l+1)^{-1}$]. The strength function is given by the slope of the curve. See text for discussion.

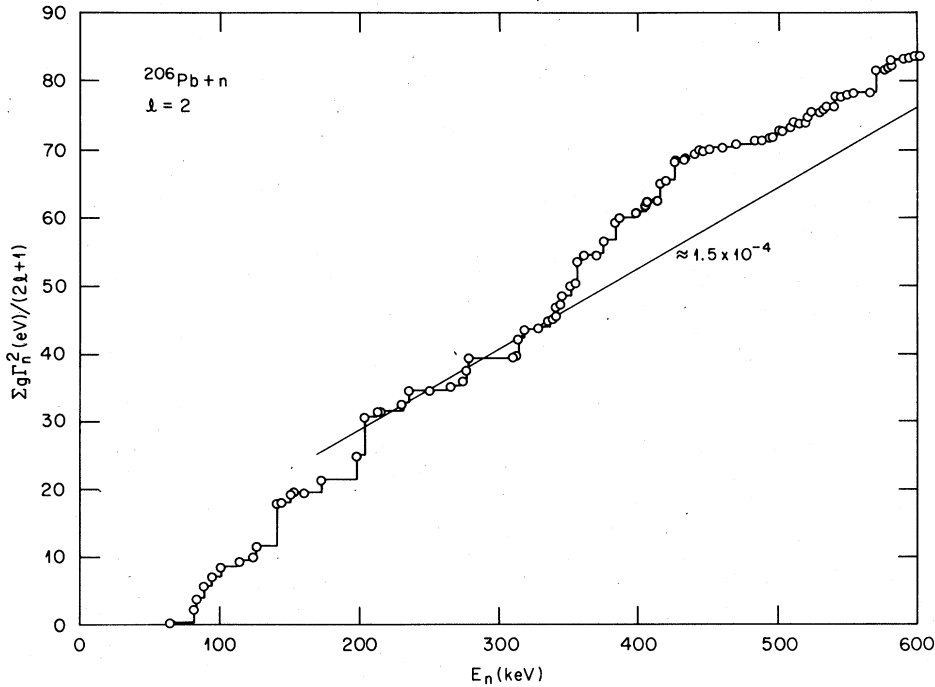


FIG. 11. Plot of the sum of reduced neutron widths $\sum g\Gamma_n^2(2l+1)^{-1}$ for d -wave resonances versus neutron energy. See text for discussion.

ways are 7.9 eV ($p_{3/2}$) and 9.7 eV ($p_{1/2}$) which would give $\Gamma_n^{3/2}/\Gamma_n^{1/2} \approx 0.8$, which is in reasonable agreement with the calculated ratio considering the uncertainties involved.

$l=2$ resonances. In Fig. 11 is shown a plot of $\sum g\Gamma_n^2(2l+1)^{-1}$ vs E for the d -wave resonances. There is an indication of a concentration of d -wave strength in the region between 350–500 keV which suggests the presence of a doorway state(s). Such a state(s) could also arise from the same particle-core excitation that is responsible for the doorway in the s -wave channel. In fact, the ($2g_{9/2}, 4^+$) particle-core excitation could give rise to levels with spins ranging from $J = \frac{1}{2} - \frac{17}{2}$. Separate plots for the $d_{3/2}$ and $d_{5/2}$ resonances do indeed indicate resonances with comparable strength in this energy interval. In addition, the $d_{3/2}$ plot shows indications of a doorway between 100–270 keV. This is in the same region³ where the $J = 1^-$ and 2^- resonances in the $^{207}\text{Pb} + n$ reaction had large reduced neutron widths, and may represent fragmentation of the $d_{3/2}$ single particle state.

Here we treat the data above 270 keV in terms of a single doorway resonance in the following analysis. For a single isolated doorway, we can express^{21,23} the sum of the reduced neutron widths as

$$\sum \Gamma_n^i = S_i E + \frac{1}{2\pi} \int_0^E \frac{1}{v_i \sqrt{E}} \frac{\Gamma^\dagger \Gamma}{[(E - E_d)^2 + (\frac{1}{2} \Gamma)^2]} dE,$$

where S_i is the strength function for the background states, Γ^\dagger is the escape width (i.e., previously denoted by Γ_n^\dagger), Γ is the total width ($\Gamma^\dagger + \Gamma_i$), and E_d is the energy of the doorway state. The escape width can be written in terms of a reduced width Γ_R^\dagger as

$$\Gamma_R^\dagger = \frac{\Gamma^\dagger}{v_i} \left(\frac{1 \text{ eV}}{E} \right)^{1/2}.$$

An initial analysis of the data showed that $\Gamma^\dagger \ll \Gamma^\dagger$, and hence $\sum \Gamma_n^i$ can be approximated as

$$\sum \Gamma_n^i = S_i E + \frac{\Gamma_R^\dagger}{2\pi} \int_0^E \frac{\Gamma^\dagger}{(E - E_d)^2 + (\frac{1}{2} \Gamma^\dagger)^2} dE.$$

This expression was used to fit the data in Fig. 11 between 250–600 keV. From this analysis we find $E_d \approx 425$ keV, $\Gamma_R^\dagger \approx 25$ eV, and $\Gamma^\dagger \approx 100$ keV. The damping width has about the same value as that found for the doorway state in the s -wave channel. It is interesting to note that we find

$$\Gamma_R^\dagger(d \text{ wave})/\Gamma_R^\dagger(s \text{ wave}) \approx 25/100,$$

where the theory would predict a value of about 0.48 for this ratio (i.e., if the radial integrals for s and d wave were the same).

Level densities. The literature pertaining to the subject of nuclear level densities is vast, and the problem of determining a level density formula is still unsolved. Many workers have attempted to fit level density data by means of a Fermi-gas model even though it has been recognized²⁴ that the latter is most likely inappropriate. Even so, they have met with reasonable success. In general, the experimental data have not been of sufficient quality to separate the observed levels by means of spin and parity. To obtain such information quantitatively over a large energy interval is difficult and requires the use of techniques which involve high-energy resolution as well as the means to determine J^π values. High resolution neutron transmission measurements have provided

an abundance of level density data including J^π values, but in general the latter have been restricted mainly to J^π for resonances formed via s -wave neutrons.

In the present study, we have identified approximately 223 resonances up to $E \approx 600$ keV. Thirteen additional resonances below 50 keV were observed²² by Mizumoto *et al.* Of these 236 resonances, 22 are s wave, 87 (19 questionable) are p wave, and 125 (61 questionable) are d wave. Included in the d waves are 20 resonances which were observed but not analyzed (see Table I). In addition, the data indicate 11 additional s -wave resonances between 600–800 keV. Even with the questionable assignments for many of these resonances, as well as the question of missing levels,

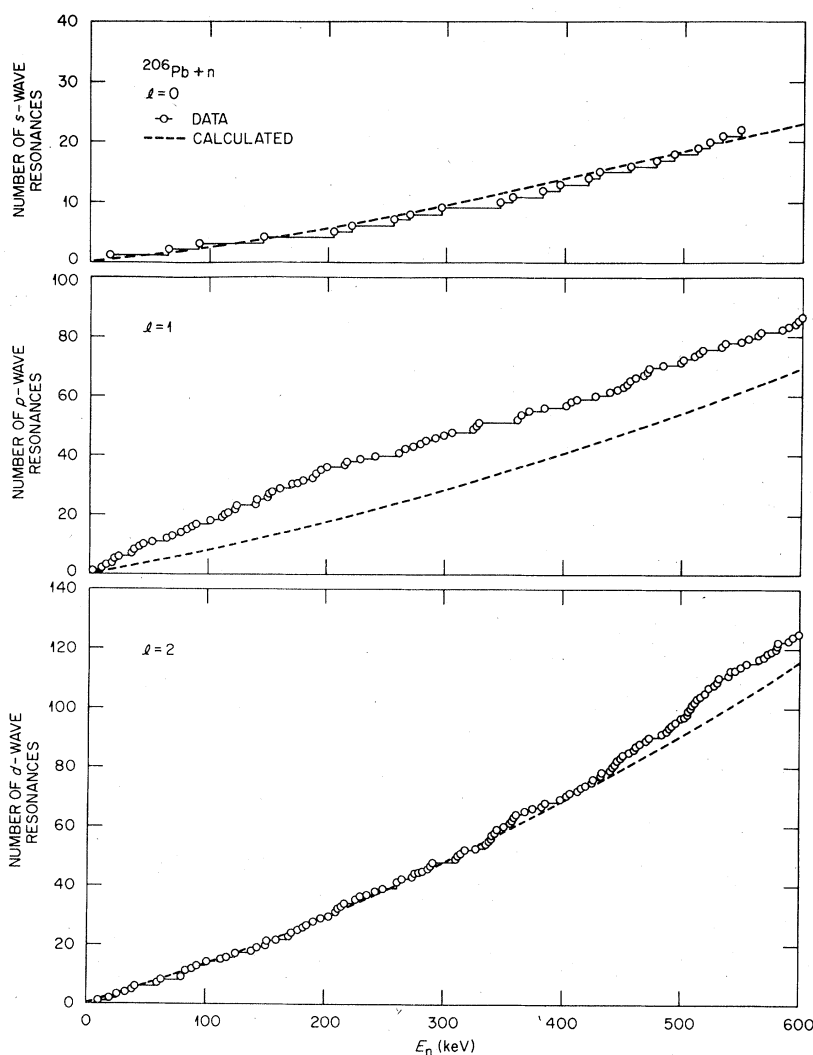


FIG. 12. Plots of the cumulative number of s -, p -, and d -wave resonances (top to bottom, respectively) versus neutron energy. The dashed lines represent calculated curves using the constant temperature model with $T = 0.9$ MeV. See text for discussion.

these data probably represent one of the best experimental sets of levels with known J^π observed thus far by means of neutron induced reactions. The only results of comparable quality have been obtained from proton studies.²⁵

The doorway state in the s -wave channel encompasses a large fraction of the energy interval under consideration. It is expected that this state will strongly affect the reduced neutron widths but has little influence on the s -wave level density. In Fig. 12(a) we plot the number of s -wave levels versus neutron energy. The slope of this curve represents the s -wave level density, which is seen to change by about 12% per 100 keV. Such a change is about what one might expect at these excitation energies if the level density followed a Fermi-gas (or constant temperature) model and had an effective nuclear temperature of about 0.9 MeV. We believe that we are missing few if any s -wave levels below 600 keV. This conclusion is based upon (a) the experimental sensitivity for detecting s -wave levels, (b) the level spacings are found to be in good agreement with a Wigner distribution, and (c) the reduced neutron widths follow a Porter-Thomas distribution reasonably well. Similar plots for p - and d -wave resonances are shown in Figs. 12(b) and 12(c), respectively.

There is an abundant literature²⁴ pertaining to the study of nuclear level density formulas. In general, the approaches have been based upon either a constant temperature model or some form of Fermi-gas model. For a constant temperature model, the density of levels is given by

$$\rho(E_x) = k e^{E_x/T},$$

where $E_x \approx S_n + E$, and k and T are constants, the latter corresponding to the nuclear temperature. The density of levels with given J^π is then taken as

$$\rho(E_x, J^\pi) = (J + \frac{1}{2}) k e^{E_x/T}.$$

The latter expression was integrated and fitted (dashed curve) to the s -wave data in Fig. 12(a). (Actually, the fit was good up to 800 keV for s waves.) This gave $T = 0.9$ MeV and $k = 0.0151$ levels/MeV. These values and the expression for $\rho(E_x, J^\pi)$ were then utilized to calculate the number of p - and d -wave resonances as a function of neutron number, and the results are shown as dashed curves in Fig. 12. The calculated curve reproduces the d -wave data rather well which tends to confirm the J dependence of $\rho(E_x, J^\pi)$ at least in the energy region under consideration, whereas the observed number of p -wave resonances is considerably larger than the calculated value and would seem to imply that the parity independence of

$\rho(E_x, J^\pi)$ is incorrect. The numbers of well established $\frac{1}{2}^-$ and $\frac{3}{2}^-$ resonances up to 605 keV are 23 and 26, respectively. There are 18 additional firm p -wave resonances and another 19 which have tentative $l=1$ assignments. Since the number of firmly established $\frac{1}{2}^-$ resonances already equals the number of $\frac{1}{2}^+$ resonances (i.e., 23 vs 22, respectively) parity independence of $\rho(E_x, J^\pi)$ would require that few if any of the additional p -wave resonances have $J = \frac{1}{2}$. Although such a possibility is unlikely, a definitive determination must await further work. However, a dependence of $\rho(E_x, J^\pi)$ upon parity would not be too surprising for a nucleus near closed shells.

Use of a Fermi-gas model in place of the constant temperature model leads to essentially the same results as described above. Here we used the simplified form of the two-fermion gas model with equidistant nucleon spacings, i.e.,

$$\rho(E_x, J^\pi) = [12\sqrt{2} \alpha^{1/4} \sigma (E_x - \delta)^{5/4}]^{-1} (J + \frac{1}{2}) \times \exp \{2[\alpha(E_x - \delta)]^{1/2}\} \exp - (J + \frac{1}{2})^2 / 2\sigma^2.$$

The parameters α , δ , and σ are assumed to be independent of energy and are related via the expressions

$$E_x - \delta \approx \alpha t^2$$

and

$$\sigma^2 = \mathcal{J}_{\text{eff}} t / \hbar^2,$$

where t is the thermodynamic temperature and \mathcal{J}_{eff} is the effective moment of inertia. To fit the s -wave data we found a set of Fermi-gas model parameters of $\alpha \approx 14$ MeV⁻¹, $\delta \approx 3$ MeV, and a value of σ^2 (i.e., spin cutoff parameter) which corresponds to about 70% of the rigid moment of inertia. The relatively large value of δ was required in order to reproduce the curvature in the plot of the number of s waves versus neutron number.

It must again be noted that any conclusions drawn from the present data must be weighed in the light of the uncertainties involved. We believe that our s -wave results clearly confirm the change in level density that would be predicted (i.e., about 12% per 100 keV) by either a constant temperature or Fermi-gas model for nuclear excitations near the neutron separation energy. Hence, one should not expect to observe straight line plots of the cumulative levels versus neutron energy over intervals greater than ≈ 100 keV as has generally been assumed by many workers in the past. The degree of confidence in the determination of the J and π dependences of $\rho(E_x, J^\pi)$ is more difficult to come by. For example, for the present case we know the lower limit for the number of p -wave resonances below 600 keV is about 68. This is very

close to the value calculated from the s -wave distribution. Hence, if all of the 19 resonances that we tentatively assigned as p wave should have other l values (which we believe unlikely), this would of course change the conclusions noted above. Finally, we point out that some of the small resonances assigned as d wave might in fact be due to higher l values, e.g., $l=3$. Hence, we conclude that before one can quantitatively test the spin and parity dependencies of the level density formula, even more definitive data will be required.

Correlation with photonuclear data. Early photonuclear measurements^{12,13} indicated the presence of a doorway state in the ground-state photon channel correlated with the s -wave neutron doorway state. However, subsequent workers^{5,10} disputed this finding. From the present work it is clear that the level density is so large that investigation of such correlations requires good energy resolution.

In this section we attempt a detailed correlation of our results with the (γ, n) data of Medsker and Jackson⁵ in hopes of examining their conclusion pertaining to the $M1$ ground-state radiative strength in ²⁰⁷Pb.

In Table I the $g_\gamma(\Gamma_{\gamma 0}\Gamma_n/\Gamma)$ values reported by Medsker and Jackson⁵ are tabulated versus neutron energy where the latter has been converted to the (n, γ) reference system. Overall, there is very good agreement between the peak energies reported in that work and our resonance energies. It should be noted that the energy resolution for the (γ, n) measurement varied from about 0.04–2.4 keV for $E=25$ –360 keV. This is about an order of magnitude poorer than that attained in this work.

Medsker and Jackson⁵ based their assignments on measurements of the relative photonuclear cross sections at 90° and 135° [i.e., $R = \sigma_{\gamma n}(90^\circ)/\sigma_{\gamma n}(135^\circ)$], which would be $R = 1.43$ for resonances with $J^\pi = \frac{3}{2}^+$, $R = 1.0$ for $J^\pi = \frac{1}{2}^\pm$, and $0.67 < R < 1.42$ for $J^\pi = \frac{3}{2}^-$. They reported $R \approx 1.0$ for most of the resonances which we have assigned as s wave (see Table I). Allen *et al.*¹⁰ in their investigation of the (n, γ) reaction report $g_n(\Gamma_\gamma\Gamma_n/\Gamma)$ values for a number of resonances below 200 keV. (The resonance energies reported in that work are about 0.5 keV higher than ours.) From a comparison of the (n, γ) and (γ, n) data we find $\Gamma_\gamma \approx \Gamma_{\gamma 0}$ for the s -wave resonances at 65.99, 92.62, and 146.31 keV. A number of peaks assigned as s wave by Medsker and Jackson⁵ seem to correspond to d -wave resonances. Of course, it should be remembered that the assignments of s -wave resonances by Medsker and Jackson⁵ were based both upon their measured $R \approx 1.0$ values and the s -wave resonances reported from transmission measurements⁸ made with much

poorer resolution.

With only a few exceptions, we find that the peaks for which Medsker and Jackson⁵ found $g_\gamma(\Gamma_{\gamma 0}\Gamma_n/\Gamma) > 1$ eV correspond to s - or d -wave resonances, and hence, the observed ground-state radiation is mainly of $E1$ rather than $M1$ character. Medsker and Jackson⁵ report $R < 1.43$ for many of the peaks in the vicinity of our d waves which no doubt indicates that they were actually observing multiplets. This would be consistent with the experimental resolution reported in the (γ, n) work and the presence of nearby p -wave resonances as can be seen in Table I.

By making use of the (n, γ) results as given by Allen *et al.*¹⁰ and requiring that $\Gamma_{\gamma 0} \leq \Gamma_\gamma$ for each resonance, one can estimate in some cases how much of the ground-state radiation might be associated with p -wave resonances. For the resonance at 124.65 keV the data of Allen *et al.*¹⁰ lead to $\Gamma_\gamma = 1.9$ eV versus $\Gamma_{\gamma 0} = 5.4$ eV for the peak observed by Medsker and Jackson.⁵ However, Allen *et al.*¹⁰ observed a resonance corresponding to that seen in our work at 125.27 keV ($l=2$) but not at 123.16 keV ($l=1$). Hence, one can clearly associate the 125.27-keV resonance with the (γ, n) peak. This resonance must then have $J^\pi = \frac{3}{2}^+$ [would likely not have been observed in (γ, n) if $J^\pi = \frac{5}{2}^+$] from which we deduce $\Gamma_\gamma = 3.7$ eV from the (n, γ) data. Thus the sum of the total radiation widths for the 124.65- and 125.27-keV resonances is then 5.6 eV which is comparable to the sum of their ground-state radiation widths. This admixture could also explain why the 124.2-keV peak in the (γ, n) reaction has $R = 1.14 \pm 0.07$ (i.e., $M1 + E2$ admixture in the 124.65-keV resonance). On this basis $\Gamma_{\gamma 0} \lesssim 1.9$ eV for the latter resonance.

Since the 140.57-keV resonance was also observed in both the (γ, n) and (n, γ) reactions, it too must have $J^\pi = \frac{3}{2}^+$ which is confirmed by our scattering data. Here we find $\Gamma_\gamma = 1.7$ eV whereas $\Gamma_{\gamma 0} = 2.1$ eV. That $\Gamma_{\gamma 0} > \Gamma_\gamma$ and $R = 1.23 \pm 0.10$ for their (γ, n) peak might suggest that it includes some contribution from the p -wave resonance at 140.95 keV. However, if the latter had $\Gamma_{\gamma 0} \approx 0.4$ eV it should have been detected in the (n, γ) experiment.

The situation appears similar for the 198.9-keV (γ, n) peak. From our assignment of $J^\pi = \frac{3}{2}^+$ to the 198.47-keV resonance we deduce $\Gamma_{\gamma 0} = 4.0$ eV versus $\Gamma_\gamma = 2.3$ eV. However, for this photopeak Medsker and Jackson⁵ found $R = 0.99 \pm 0.06$ which again suggests the presence of a multiplet. Although Allen *et al.*¹⁰ did not tabulate widths for resonances greater than 198.4 keV, additional resonances are present in their data (see their Fig. 7). In particular, there appears to be a resonance near 200 keV with about one-fourth the strength of the 198.4-keV resonance. We suggest

that our p -wave resonance at 200.69 keV is probably also included in the (γ, n) peak, and would therefore have $\Gamma_{\gamma 0} < 1.3$ eV. In general, the relative cross section ratios (i.e., R) as measured by Medsker and Jackson⁵ agree fairly well with our assigned J^π above 200 keV. Their value of $R = 1.09 \pm 0.10$ for the 276.7-keV peak may imply a multiplet (perhaps including the 274.63-keV resonance).

The uncertainties in the data do not permit one to determine with complete confidence the $M1$ radiative strength in this region of excitation of ^{207}Pb . However, using the results tabulated in Table I in addition to those for three resonances below 25 keV reported by Bowman *et al.*,¹¹ we can set a conservative upper limit of $\sum g_\gamma \Gamma_{\gamma 0} \Gamma_n / \Gamma < 23.7$ eV [or on average $B(M1)^\dagger \langle 8 \mu_0^2 \rangle$] for the neutron energy interval $E = 3 - 600$ keV which is less than 40% of the strength designated by Medsker and Jackson⁵ as $M1$. Our sum even includes some resonances assigned as possible d wave in Ref. 5.

It is instructive to compare this sum of ground-state radiation widths with that found for ^{208}Pb . Essentially no $M1$ radiative strength has yet been found in ^{208}Pb between 6738–7368 keV. Between 7368 (threshold) and 7750 keV, $\sum g_\gamma \Gamma_{\gamma 0} \Gamma_n / \Gamma \approx 20$ eV,¹⁻³ which on average is about 5 eV per 100 keV. However, about half of this (i.e., ≈ 11 eV) is located within the p -wave doorway state¹ at 7494 keV. From the above, we see that for ^{207}Pb between 6739 and 7341 keV one finds the average value $\sum g_\gamma \Gamma_{\gamma 0} \Gamma_n / \Gamma \approx 4$ eV per 100 keV. If the actual situation were to tend toward this upper limit, and if one were to consider ^{207}Pb to act as a ^{208}Pb core plus an inert $p_{1/2}$ hole, then this would suggest that ^{208}Pb would have an $M1$ radiative strength of $\sum g_\gamma \Gamma_{\gamma 0} \Gamma_n / \Gamma \approx 2$ eV per 100 keV in this same region of excitation. (The weak-coupling model would predict that the sum of the $M1$ radiation widths for ^{207}Pb would be twice that for ^{208}Pb .) Such $M1$ strength²⁶ has not as yet been identified in the bound-state region of ^{208}Pb .

V. CONCLUSIONS

In this work we have examined the $^{206}\text{Pb} + n$ reaction by means of high resolution neutron transmission and scattering measurements. Para-

meters for about 223 resonances formed by s -, p -, and d -wave neutrons have been determined. Neutron strength functions have been deduced which indicate the presence of doorway states. The latter seem to arise from particle-core excitations, e.g., $(g_{9/2}, 4^*)$ and $(d_{5/2}, 3^-)$. The energies of the $p_{1/2}$ and $p_{3/2}$ doorway states agree well with the results found in a study³ of the $^{207}\text{Pb} + n$ reaction. A resonance in the d -wave neutron strength function was found at about the same energy as the s -wave doorway state. It is suggested that this originates from a recoupling of the same particle-core excitation that is responsible for the s -wave doorway state.

A plot of the cumulative number of s -wave resonances versus neutron energy could be reproduced fairly well using a constant temperature level density formula, $\rho(E_x) = ke^{E_x/T}$ with $T = 0.9$ MeV. Assuming the J -dependent level density goes as $\rho(E_x, J) = (2J + 1)\rho(E_x)$, this expression also reproduced the cumulative number of d -wave resonances, but it underestimated the number of p -wave resonances. However, uncertainties as to the J values for a number of resonances prevented a strong statement as to the J and π dependence of the level density formula.

This work clearly shows that the $M1$ radiative strength in ^{207}Pb is considerably less than has been reported⁵ previously. More accurate measurements of the $^{207}\text{Pb}(\gamma, n)$ reaction would be desirable to enhance further investigation of this problem.

ACKNOWLEDGMENTS

The authors would like to thank Mr. John Shriner for his extensive aid with the data analysis. Discussions with Dr. J. McGrory pertaining to theoretical aspects of this paper proved extremely valuable. Dr. C. H. Johnson kindly provided computer programs for calculating level densities, and Dr. R. R. Winters programs for calculating Porter-Thomas and Wigner distributions. This work would not have been successful without the support of the ORELA staff. This research was sponsored by the Division of Basic Energy Science, U.S. Department of Energy under Contract No. W-7405-eng-26 with Union Carbide Corporation.

¹D. J. Horen, N. W. Hill, and J. A. Harvey, Phys. Rev. Lett. **38**, 1344 (1977).

²S. Raman, M. Mizumoto, and R. L. Macklin, Phys. Rev. Lett. **39**, 598 (1977).

³D. J. Horen, N. W. Hill, and J. A. Harvey, Phys. Rev.

C **18**, 722 (1978).

⁴D. J. Horen, G. F. Auchampaugh, and J. A. Harvey, Phys. Lett. **79B**, 39 (1978).

⁵L. R. Medsker and H. E. Jackson, Phys. Rev. C **9**, 709 (1974).

- ⁶E. G. Bilpuch, K. K. Seth, C. D. Bowman, R. H. Tabony, R. C. Smith, and H. W. Newson, *Ann. Phys. (N.Y.)* **14**, 387 (1961).
- ⁷R. L. Macklin, P. J. Pasma, and J. H. Gibbons, *Phys. Rev.* **136**, B695 (1964).
- ⁸J. A. Farrell, G. C. Kyker, Jr., E. G. Bilpuch, and H. W. Newson, *Phys. Lett.* **17**, 286 (1965).
- ⁹J. A. Biggerstaff, J. R. Bird, J. H. Gibbons, and W. M. Good, *Phys. Rev.* **154**, 1136 (1967).
- ¹⁰B. J. Allen, R. L. Macklin, C. Y. Fu, and R. R. Winters, *Phys. Rev. C* **7**, 2598 (1973); B. J. Allen, R. L. Macklin, R. R. Winters, and F. Y. Fu, *ibid.* **8**, 1504 (1973).
- ¹¹C. D. Bowman, B. L. Berman, and H. E. Jackson, *Phys. Rev.* **178**, 1827 (1969).
- ¹²R. J. Baglan, C. D. Bowman, and B. L. Berman, *Phys. Rev. C* **3**, 672 (1971).
- ¹³R. J. Baglan, C. D. Bowman, and B. L. Berman, *Phys. Rev. C* **3**, 2475 (1971).
- ¹⁴D. C. Larson, C. H. Johnson, J. A. Harvey, and N. W. Hill, Oak Ridge National Laboratory Report No. ORNL/TM-5612, 1976 (unpublished).
- ¹⁵A. M. Lane and R. G. Thomas, *Rev. Mod. Phys.* **30**, 257 (1958).
- ¹⁶G. F. Auchampaugh, Los Alamos Scientific Laboratory Report No. LA-5473-MS, 1974 (unpublished).
- ¹⁷F. G. Perey (private communication).
- ¹⁸J. M. Blatt and L. C. Biedenharn, *Rev. Mod. Phys.* **30**, 257 (1958).
- ¹⁹W. E. Kinney (private communication).
- ²⁰F. T. Seibel, E. G. Bilpuch, and H. W. Newson, *Ann. Phys. (N.Y.)* **69**, 451 (1972).
- ²¹W. P. Beres and M. Divadeenam, *Phys. Rev. Lett.* **25**, 596 (1970). See also M. Divadeenam, W. B. Beres, and H. W. Newson, *Ann. Phys. (N.Y.)* **80**, 231 (1973); M. Divadeenam and W. P. Beres, in *Statistical Properties of Nuclei*, edited by J. Garg (Plenum, New York, 1972) p. 579.
- ²²M. Mizumoto, S. Raman, R. L. Macklin, G. G. Slaughter, J. A. Harvey, and J. H. Hamilton, *Phys. Rev. C* **19**, 335 (1979).
- ²³H. Feshbach, A. K. Kerman, and R. H. Lemmer, *Ann. Phys. (N.Y.)* **41**, 230 (1967).
- ²⁴See, for example, J. R. Huizenga and L. G. Moretto, *Annu. Rev. Nucl. Sci.* **22**, 427 (1972).
- ²⁵E. G. Bilpuch, N. H. Prochnow, R. Y. Cusson, H. W. Newson, and G. E. Mitchell, *Phys. Lett.* **35B**, 303 (1971); E. G. Bilpuch, A. M. Lane, G. E. Mitchell, and J. D. Moses, *Phys. Rep.* **28C**, 145 (1976).
- ²⁶D. J. Horen, R. T. Kouzes, D. Mueller, F. Galaprice, and R. P. Hall, *Phys. Rev. C* **19**, 549 (1979).